THEORETICAL FOUNDATIONS OF 3D SCALAR FIELD VISUALIZATION

Mohammed Mostefa Mesmoudi
Department of Mathematics, University of Mostaganem, Po. Box 227, Route BelHacel, Mostaganem 27000, Algeria

Leila De Floriani
Department of Computer Science, University of Genova, Via Dodecaneso n 35, 16146 Genova, Italy

Paolo Rosso
Department of Information Systems and Computation, Polytechnic University of Valencia
Camino de Vera s/n, 46022 Valencia, Spain

Keywords: 3D Visualization, geometric modeling, morphology extraction, image segmentation, watershed transform, multiresolution.

Abstract: In this paper we introduce two novel technics that allow for a three dimensional scalar field to be visualized in the three dimensional space R^3. Many applications are possible especially in medicine imagery. New multiresolution models can be build based our techniques. Moreover, we show that these two visualization techniques allow the extraction of morphological features of the space and that may not be captured by classical methods.

1 INTRODUCTION

In many applications of computer graphics (e.g., medicine imaging) the visualization of scalar fields is a basic tool to explore and understand the structure of the field. Visualization of 3D scalar fields needs an additional dimension to be achieved. This is impossible to do in R^3 from the Cartesian point of view since our visual perception is limited to three parameters. To overcome this problem, we need to tackle the problem from a different point of view.
Smooth Morse theory is the basic tool used to extract morphological features of a domain endowed with a scalar field (Smale, 1960). The domain is decomposed into stable and unstable components. Stable components are associated with minima, while unstable components are associated with maxima. In the discrete case algorithms have been proposed to extract morphological features with similar properties as in Morse theory. A large part of such techniques deal with 2D scalar fields case, see, for instance, (Bajaj et al., 1998), (Bajaj and Shikore, 1998), (Edelsbrunner et al., 2001), (J.Toriwaki and Fukumura, 1975), (Nackman, 1984), (Peucker and Douglas, 1975), (Watson et al., 1985). The watershed transform introduced by Vincent et al. in (Vincent and Soille,), for 2D scalar fields considers the graphical representation of a 2D scalar field as a surface that will be immersed progressively in water. Catchment basins, which correspond to stable Smale decomposition in Morse theory, are constructed and surface segmentation is, hence, performed. Very few papers deal with 3D (and 4D) scalar fields. This is due to difficulty of applying, in the discrete, Morse theory to 3D (and 4D)scalar fields. In (H. Edelsbrunner, 2003), an algorithm for the construction of Smale-decomposition for linear piece-wise linear functions on a three dimensional domain is presented. Mangan et al., gave in (Mangan and Whitaker, 1999) a watershed algorithm that segments a 3D surface into patches. Their algorithm is based on the total curvature of the surface approximated at the vertices of the mesh approximating the surface.

Here, we present two coupled novel techniques that allow visualizing 3D scalar fields in the Euclidean three-dimensional space. These novel techniques, that we call *AUBL* and *PGR*, are based on some fundamental geometric properties of surfaces and

Mostefa Mesmoudi M., De Floriani L. and Rosso P. (2007).
THEORETICAL FOUNDATIONS OF 3D SCALAR FIELD VISUALIZATION.
In *Proceedings of the Second International Conference on Computer Vision Theory and Applications*, pages 69-77
DOI: 10.5220/0002065300690077

on their embedding the Euclidean three-dimensional space. *AUBL* and *PGR* visualization techniques have the advantage of representing a 3D scalar field in a natural and intuitive way and allow extracting morphology features of the field that may not be captured by classical methods. Hence, we obtain a natural generalization, to 3D scalar fields, of the *watershed transform*. In addition, *AUBL* and *PGR* techniques provide a new approach to study a 3D scalar field using additional tools like curvature of the surface or of the field, and dependencies under elementary transformation (e.g., time evolution of a pathology) and that were not possible with classical methods. *AUBL* and *PGR* can be used as a support for data mining visualization of 4D scalar fields. Study of 4D scalar fields goes beyond the scope of this paper whose aim is to present the mathematical foundations of *AUBL* and *PGR* techniques. Many applications of *AUBL* and *PGR* are possible in 3D visualization, especially in medical imaging New multi-resolution models based on *AUBL* technique can be build. We will discuss this possibility in the paper. Roughly speaking, the *AUBL* technique represents the scalar field as an *atmosphere* over the domain and *PGR* represents the depth of the upper layer of the atmosphere.

The remainder of this paper is organized as follows. In the next Section we present some background notions related to the basic mathematical notions needed in this paper. In Section 3, we present the fundamental geometric property from which we derive the *AUBL* and *PGR* visualization algorithms. We will discuss how algorithms *AUBL* and *PGR* can be used to extract and visualize morphological features of a field that may not be detected through other classical techniques. In Section 4, we describe how *AUBL* visualization technique can generalize the watershed transform to extract the morphological feature. In the last Section, we draw some concluding remarks and we discuss our ongoing work.

2 BACKGROUND

In this Section, we present the basic mathematical notions that we need to develop the paper material.

2.1 Geometry and Topology of 2-Manifolds

Two dimensional manifolds (without boundary) are surfaces that are locally diffeomorphic to discs of R^2. Around any point p of a surface S, one can find a neighborhood $\mathcal{U}$ of p and a diffeormorphism ϕ that maps a disc in R^2 on $\mathcal{U}$. At each point p of a surface S, a tangent plane T_pS is defined and thus a normal vector $\overrightarrow{N_p}$ to S at point p can be drawn. Vector $\overrightarrow{N_p}$ generates a 1-dimensional vectorial space $<\overrightarrow{N_p}>$. Hence, the Euclidean 3-dimensional space R^3 is retrieved in the direct sum $T_pS \oplus <\overrightarrow{N_p}>$ of vectorial spaces T_pS and $<\overrightarrow{N_p}>$, see Figure 1.

If the surface S is described by an equation

Figure 1: A surface with its tangent plane and normal vectorial space at a point.

$f(x,y,z) = 0$ (e.g., $x^2+y^2+z^2-1=0$ for the unit sphere), then coordinates of the normal vector $\overrightarrow{N_p}$ to S at a point p are given by the partial derivatives $(\frac{\partial f}{\partial x}(p), \frac{\partial f}{\partial y}(p), \frac{\partial f}{\partial z}(p))$. The tangent plane is described by the equation $\frac{\partial f}{\partial x}(p)(x-x_p) + \frac{\partial f}{\partial y}(p)(y-y_p) + \frac{\partial f}{\partial z}(p)(z-z_p) = 0$. If surface S is described by a parametric relations $S = \{(x(t,s),y(t,s),z(t,s)) : (t,s) \in D \subset R^2\}$, then tangent plane is generated by the two vectors $\overrightarrow{V_p} = (\frac{\partial x}{\partial t}(t_0,s_0), \frac{\partial y}{\partial t}(t_0,s_0), \frac{\partial z}{\partial t}(t_0,s_0))$ and $\overrightarrow{V'_p} = (\frac{\partial x}{\partial s}(t_0,s_0), \frac{\partial y}{\partial s}(t_0,s_0), \frac{\partial z}{\partial s}(t_0,s_0))$ with $p = (x(t_0,s_0),y(t_0,s_0),z(t_0,s_0))$. Then the normal vector $\overrightarrow{N_p}$ is equal to the vectorial product $\overrightarrow{V_p} \bigwedge \overrightarrow{V'_p}$ whose coordinates are given by $(\frac{\partial y}{\partial t}(t_0,s_0)\frac{\partial z}{\partial s}(t_0,s_0) - \frac{\partial z}{\partial t}(t_0,s_0)\frac{\partial y}{\partial s}(t_0,s_0); -\frac{\partial x}{\partial t}(t_0,s_0)\frac{\partial z}{\partial s}(t_0,s_0) + \frac{\partial z}{\partial t}(t_0,s_0)\frac{\partial x}{\partial s}(t_0,s_0); \frac{\partial x}{\partial t}(t_0,s_0)\frac{\partial y}{\partial s}(t_0,s_0) - \frac{\partial y}{\partial t}(t_0,s_0)\frac{\partial x}{\partial s}(t_0,s_0))$. For more details, we refer to any book of differential geometry (e.g., (Berger and Gostiaux, 1972), (Spivak, 1979)).

Two surfaces are said be topologically equivalent if they are homeomorphic. Algebraic topology classifies compact surfaces by their genus and orientability, see (Massey, 1977). The genus g is the number of handles in a surface. A topological sphere S^2 has null genus since it has no handle, while a torus T^2 has genus 1, since it has exactly one handle. To obtain surfaces of a higher genus $g \geq 2$, we consider the connected sum of g tori ($T^2 \# T^2 \# \ldots \# T^2$). The connected

sum is defined by the quotient space of an equivalence relation that identifies (i.e., glue) the boundary points of two holes created on two consecutive tori. In Figure 2, we give an illustration of such surfaces with genus 0, 1, 2 or 3. A compact surface with non empty boundary components can be obtained from the previous described surfaces by cutting along closed curves. In the remainder of this paper we consider only orientable surfaces.

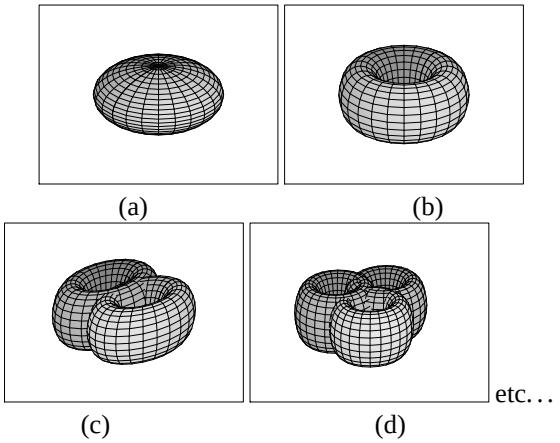

Figure 2: Surfaces of genus 0 in (a), 1 in (b), 2 in (c) and 3 in (d), and so on.

2.2 Morse Theory

A *Morse function* on a manifold M is a C^2-differentiable real-valued function f defined on M such that its *critical* points are non-degenerate (Milnor, 1963). This means that the Hessian matrix $Hes_P f$ of the second derivatives of f at any point $P \in R^d$ on which the gradient of f vanishes ($Grad_P f = 0$) is non-degenerate ($Det(Hes_P f \neq 0$). Morse (Milnor, 1963) has proven that there exists a local coordinate system $(y^1,...,y^n)$ in a neighborhood U of any critical point P, with $y^j(P) = 0$, for all $j = 1,\ldots,n$, such that the identity

$$f = f(P) - (y^1)^2 - ... - (y^\imath)^2 + (y^{\imath+1})^2 + ... + (y^n)^2$$

holds on U, where $\imath$ is the number of negative eigenvalues of $Hes_P f$, and it is called the *index* of f at P. The above formula implies that the critical points of a Morse function are isolated. This allows us to study the behaviour of f around them, and to classify their nature according to the signs of the eigenvalues of the Hessian matrix of f. If the eigenvalues are all positives, then the point P is a *strict local minimum* (a pit). If the eigenvalues are all negatives, then P is a *strict local maximum* (a peak). If the index $\imath$ of f at point P is different from 0 and n, then the point P is neither a minimum nor a maximum, and, thus, it is called an *$\imath$-saddle* point (a pass).

The decomposition of the manifold domain associated with f, introduced by Thom (Thom, 1949) and followed by Smale (Smale, 1960) is based on the study of the growth of f along its integral curves. An integral curve is a curve which is every where tangent to the gradient vector field. Integral curves originating from a critical point of index $\imath$ form a $\imath$-cell C^s, called a *stable manifold*. In the same way integral curves converging to a critical point of index $\imath$ form a dual $(n-\imath)$-cell C^u, called an *unstable manifold*. Stable manifolds are pairwise disjoint and decompose the field domain M into open cells, (see Figure 3). The cells form a complex, as the boundary of every stable manifold is the union of lower dimensional cells. Similarly, the unstable manifolds decompose M into a complex dual to the complex of stable manifolds. Integral curves connecting saddles to other critical points are called *separatrices*.

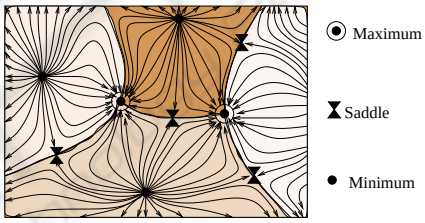

Figure 3: Decomposition of a domain into four stable 2-manifolds.

3 3D SCALAR FIELDS VISUALIZATION

By *3D scalar field* we mean a scalar field defined on any smooth surface embedded in R^3. Such surfaces may have non-null genus, may contain boundary components, may be compact, open, etc...
The basic idea underlying our new technique is to use a fundamental geometric property of the representation of 2D scalar fields in the 3D Euclidean space. Let us discuss first the graphical representation of a scalar field f defined on a domain D of R^2. The graphical representation of f over D is a surface S defined as

$$S = \{(x,y,z) : (x,y) \in D \text{ and } z = f(x,y)\} \qquad (1)$$

The domain D in R^3 is embedded onto a set $\tilde{D} = \{(x,y,0) : (x,y) \in D\}$ and a point $p(x,y)$ in D is sent

to point $\tilde{p}(x,y,0)$ in $\tilde{D}$. Also, domain $\tilde{D}$ has a parameterization through points of D. Hence, function f can be seen as a 3D scalar field $\tilde{f}$ defined on $\tilde{D}$ by : $\tilde{f}(\tilde{p}) = f(p)$. In Figure 4, we illustrate such situation.

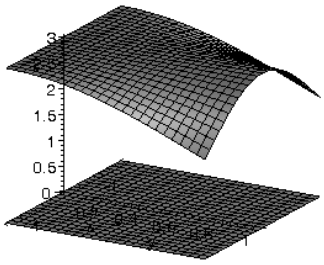

Figure 4: Graphic representation of $f(x,y) = \tilde{f}(x,y,0) = cos(xy)$ over the Domain $D = [-\pi/2,\pi/2] \times [0,\pi/3] \simeq [-\pi/2,\pi/2] \times [0,\pi/3] \times \{0\} = \tilde{D}$.

Property 1 (The first key Property.) *For a given point $\tilde{p}$ in $\tilde{D}$, vector $\overrightarrow{\tilde{p}\tilde{f}(\tilde{p})}$ is normal to $\tilde{D}$ and $\| \overrightarrow{\tilde{p}\tilde{f}(\tilde{p})} \| = | f(\tilde{p}) |$.*

This is due to the fact that the canonical basis of R^3 is orthonormal and $(0,0,f(x,y))$ are the coordinates of vector $\overrightarrow{\tilde{p}\tilde{f}(\tilde{p})}$.
Generalizing the idea in property 1, we can give a first graphical representation of 3D scalar fields. Let S be an embedded smooth surface in R^3 and f be a scalar field defined on S. The graphical representation of function f would be a subset of R^4 defined by

$$G = \{(x,y,z,t) : (x,y,z) \in S \text{ and } t = f(x,y,z)\} \quad (2)$$

Since we cannot visualize items in R^4, Property 1 allow us to visualize both S and its image by f in R^3 as in Figure 4.
First Visualization principle.

Definition 1 *Let $\overrightarrow{N_p}$ be the unit normal vector of S at point p. The graphical representation of scalar field f over S is the surface $\mathcal{S} \subset R^3$ defined by:*

$$\mathcal{S} = \{p + f(p)\overrightarrow{N_p} : p \in S\} \quad (3)$$

To represent the image of point $p \in S$, the previous definition associates p with the point $\tilde{f}(p) := p + f(p)\overrightarrow{N_p}$. Then, vector $\overrightarrow{p\tilde{f}(p)}$ is normal to S at p and $\| \overrightarrow{p\tilde{f}(p)} \| = | f(p) |$ Thus, Property 1 is satisfied. The graphical representation of function f defines an *atmosphere layer* over surface S. The thickness of the layer is given by the function values. As an example, the graphical representation of a constant function over a sphere is a larger sphere with the same center and in which the radius is augmented by the constant value of the function.

Definition 2 *When surface S is included in the interior space bounded by $\mathcal{S}$ we say that S has a positive f-atmosphere. When the reverse holds, we say that S has a negative f-atmosphere.*

When the new surface $\mathcal{S}$ is topologically equivalent to S, we can always inflate or deflate surface $\mathcal{S}$ (without losing the perpendicularity property) so that $\mathcal{S} \cap S = \emptyset$ and obtain positive, or negative atmosphere following the need of the user to get a best representation scheme. *Inflation* (resp: *deflation*) can be performed by translating $\tilde{f}(p)$ in the direction of the normal vector $\overrightarrow{N_p}$ by a constant positive (resp. negative) value. Formal definitions of inflation and deflation are given in section 4. To avoid self-intersections of $\mathcal{S}$ due to limitation of available space in the interior of eventual handles of the surface S, we can change the scale of the normal vector $\overrightarrow{N_p}$ by a multiplicative smaller constant value.
When the topology equivalence between S and $\mathcal{S}$ is not satisfied, we can only deflate $\mathcal{S}$ to include it in the interior space of S and, hence, obtain a negative atmosphere. In Figure 6, we illustrate the above situation for the unit sphere $x^2 + y^2 + z^2 = 1$ with a negative atmosphere corresponding to the function $f(x,y,z) = x^2 - y^2 - 1$.

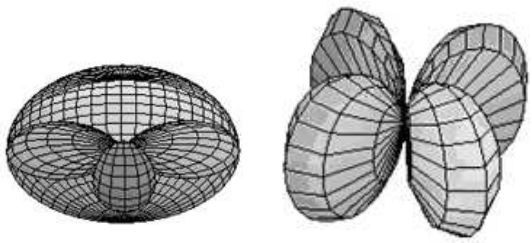

(a) (b)

Figure 5: In (a), a plane section representing the unit sphere with a negative atmosphere defined by a function $f(x,y,z) = x^2 - y^2 - 1$. In (b), the visualization of $\mathcal{S}$ corresponding to $\tilde{f}$.

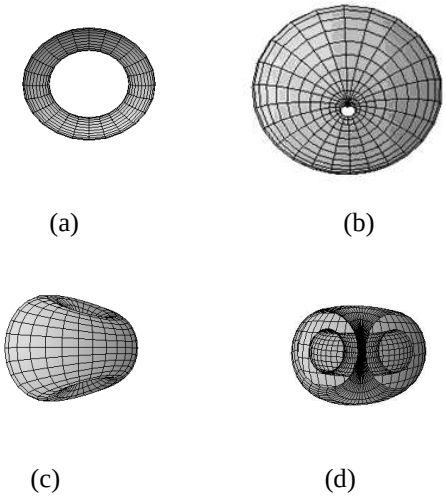

(a) (b)

(c) (d)

Figure 6: In (b)and (c): The graphical representation of *Ox*-height function $f(x,y,z) = x$ of a torus T^2 (in (a)) whose revolution axis is *Oz*. In (d), we represent a section of the height function representation: The torus and its f-atmosphere are Shown.

Definition 3 *Under such assumptions, we call the graphical representation $\mathcal{S}$ of f, the atmosphere upper bound layer $(AUBL)$ of the pair (S, f).*

In Figure 6, we illustrate the atmosphere of *Ox*-height function defined on a torus T^2 whose revolution axis is *Oz* (i.e., $f(x,y,z) = x$ for all points $(x,y,z) \in T^2$).

Second Visualization Principle.
AUBL visualization can be completed by a second visualization technique based on a graph representation of f over flat subset $D \in R^2$. This can be realized by composing f with a (local) coordinates system on S. Of course, this second visualization does not represent directly f over S, but it has some advantages:

- This representation provides additional information on the morphology of the surface that can be easily captured by the different existing techniques since it is based on 2D scalar field visualization.
- The AUBL visualization technique described above depends on the geometry of surface S. Hence, a negatively (resp. positively) curved hump on S may produce a negatively (resp. positively) curved hump on $\mathcal{S}$. Then function f may have a decreasing (resp. increasing) appearance, while, in reality, f has the opposite growth. To compensate this issue, we consider the growth of f over a flat domain of R^2. Composing f with ϕ and then representing the resulting function over D solves this issue.
  From an other point of view, the above discussed humps that appear on $\mathcal{S}$ represent interesting regions related to the morphology of the surface and that may correspond to *some kind of critical* points of the vector function $\tilde{f}$ and/or f. Thus, additional morphology information is captured by *AUBL* visualization that cannot be seen by standard tools.

Let $\{\phi(t,s) = (x(t,s), y(t,s), z(t,s)) : (t,s) \in D\}$ a local (or a global) parameterization of S over a domain $D \in R^2$.

Definition 4 *We call the visualization of $f \circ \phi$ over D by the parametric growth representation (PGR) of f over S.*

Hence, a complete understanding of f will be achieved by coupling together both visualizations *AUBL* and *PGR*.

In Figure 7, we provide an illustration of (*AUBL*, *PGR*)-visualizations of the (Ox)-height scalar field defined on torus T^2 parameterized by (t,s) where t is the angle between axis (Ox) and $\overrightarrow{Op'}$ where p' is the projection a current point p on T^2. Parameter s is the angle between axis (Oz) and $\overrightarrow{Op}$. The *PGR* representation shows that setting parameter $s = s_0$, function $f \circ \phi(t, s_0))$ increases, reaches a maximum and then decreases. Similar behaviour happens by fixing first t.

In the following example, we consider the case of a function which is not Morse with two degenerated points. We will show how *PGR* visualization technique can be applied to extract 6 critical points on a surface. In Section 4, we will show how *AUBL* visualization technique can be applied to retrieve the same critical points with the critical net in addition.
Example. Let us consider function $f(x,y,z) = x^2 - y^2$ defined on the unit sphere S^2. Gradient vector field at any point $p = (x,y,z) \in R^3$ is given by $Grad_p f = (2x, -2y, 0)$. The gradient field vanishes on the set $\{(0,0,z) :\in R\}$. The Hessian matrix $Hes_p f$ of f at point p is generated by column vectors $(2,0,0)$, $(0,-2,0)$ and $(0,0,0)$. Matrix $Hes_p f$ is clearly degenerate at any point $p \in R^3$. Hence f is not a Morse function. Thus, we can not apply techniques of Morse theory to study f.
Let us parameterize the unit sphere with it spherical coordinates $x = cos(t)sin(s)$, $y = sin(t)sin(s)$ and $z = cos(s)$, where $t \in [0, 2\pi]$ is the angle in (Oxy)-plane attached to the (Ox)-axis. Parameter $s \in [0, \pi]$ is the angle attached to (Oz)-axis. A simple computation gives $\tilde{f}(t,s) = f(x(t,s), y(t,s), z(t,s)) =$

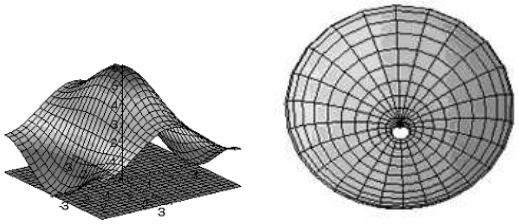

(a) (b)

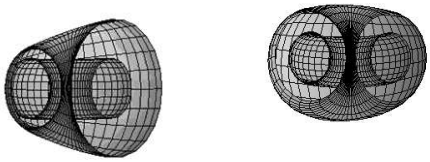

(c) (d)

Figure 7: In (a) the *PGR* and, in (b), the *AUBL* visualizations of *Ox*-height function $f(x,y,z) = x$ of torus $T^2 = \{(x(t,s),y(t,s),z(t,s)) : x(t,s) = (2 + cos(s))cos(t); y(t,s) = (2 + cos(s))sin(t); z(t,s) = sin(s) : (t,s) \in [-\pi,\pi]^2\}$. In (c), an atmosphere section at $t = 0$ and at $t = \pi$. In (d), an atmosphere section at $t = -\pi/2$ and at $\pi/2$.

$cos(2t)sin^2(s)$. The gradient vector field of $\tilde{f}$ at a point $u = (t,s)$ is given by

$$Grad_u\tilde{f} = (-2sin(2t)sin^2(s), cos(2t)sin(2s)).$$

The gradient of $\tilde{f}$ vanishes on the set $Crit\,\tilde{f} = \{(t,0),(t,\pi) : t \in [0,2\pi]\} \cup \{(0,0),(\pi/2,\pi/2),(\pi,\pi/2),(3\pi/2,\pi/2\}$. On the unit sphere, points in the first set of $Crit\,\tilde{f}$ of type $(t,0)$ correspond to the north pole $(0,0,1)$, and to the south pole $(0,0,-1)$ for points of type (t,π). Points in the second set of $Crit\,\tilde{f}$ corresponds respectively to $(1,0,0)$, $(0,1,0)$, $(-1,0,0)$ and $(0,-1,0)$.

The Hessian matrix of $\tilde{f}$ is generated by vectors $(-4cos(2t)sin^2(s), -2sin(2t)sin(2s))$ and $(-2sin(2t)sin(2s), 2cos(2t)cos(2s))$. Simple computation implies that $Hes_u\tilde{f}$ is degenerate for points of type $(t,0)$ and (t,π) that corresponds to north and south poles of the sphere. For the other four points, the Hessian $Hes_u\tilde{f}$ is non degenerate and has determinant equal to 8 (≥ 0) at each point. This implies that each point in $\{(0,0),(\pi/2,\pi/2),(\pi,\pi/2),(3\pi/2,\pi/2\}$ is either a maximum or a minimum. Thus maxima and minima of f on the unit sphere correspond to $(1,0,0)$, $(0,1,0)$, $(-1,0,0)$ and $(0,-1,0)$. A simple computation gives a maximal value 1 of f at points $(1,0,0)$ and $(-1,0,0)$ and a minimal value -1 of f at points $(0,1,0)$ and $(0,-1,0)$. Hence, north and south poles of the sphere are degenerate saddles and f vanishes on them ($f(0,0,1) = f(0,0,-1) = 0$). The *PGR* visualization of function f is illustrated in Figure 8(a).

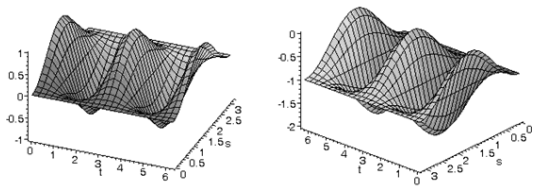

(a) (b)

Figure 8: In (a), *PGR* visualization of the function $f(x,y,z) = x^2 - y^2$ over the unit sphere. Maxima and minima appear alternatively. There are two minima and one maximum in the interior of the surface. Two maxima appear on the boundary segments $t = 0$, $t = 2\pi$ but they correspond to the same point on the unit sphere. Function $f \circ \phi$, has a constant value on segments $s = 0$, $s = \pi$. Points on these boundary segments are critical, they correspond all to the north or the south pole. In (b), the *PGR* visualization of the function $f(x,y,z) = x^2 - y^2 - 1$. The shapes of surfaces in (a) and in (b) are identical. This is not the case with *AUBL* visualization technique, see Figure 9(a) and (c).

4 MORPHOLOGY EXTRACTION BASED ON *AUBL* INFLATION/DEFLATION

The distance between a point p and its image (on *AUBL*, *PGR* or in the standard cartesian case) is given by $\mid f(p) \mid$. Points for which this distance is minimal correspond to minima and points for which this distance is maximal correspond to maxima. In this section we will give a method that extracts those critical points with saddle and the critical net on surface S associated with function f. To begin, let us give a formal definition of inflation and deflation.

Definition 5 *Suppose that normal vectors $\overrightarrow{N_p}$ are directed towards the exterior of S. Inflation process is a dynamical system $Inflat : \mathcal{S} \times [0,+\infty[\rightarrow R^3$ that associates a pair $(\tilde{f}(p),t)$ with $Inflat(\tilde{f}(p),t) = \tilde{f}(p) + t\overrightarrow{N_p}$.*

Deflation process is a dynamical system $Deflat : \mathcal{S} \times]-\infty,0] \rightarrow R^3$ that associates a pair $(\tilde{f}(p),t)$ with $Deflat(\tilde{f}(p),t) = \tilde{f}(p) - t\overrightarrow{N_p}$.

For each instant t_0, $Inflat(\mathcal{S},t_0)$ (resp. $Deflat(\mathcal{S},t_0)$) is a surface $\mathcal{S}_{t_0}$ obtained from $\mathcal{S}$ by translating all points $\tilde{f}(p)$ along vectors $\overrightarrow{N_p}$ by constant value

t_0. In Section 3, we have seen that inflation and deflation of the atmosphere permit to get positive and negative atmospheres over the surface S. This inflation/deflation process has an important property in capturing the morphology of surface S. This is given by

Property 2 (The second key Property). *While performing an inflation/deflation, imprints of crossing surface S at a given time t_0 defines level sets $S \cap \mathcal{S}$ of f over S at moment t_0.*

Proof. At instant t_0, intersection of surface $\mathcal{S}_{t_0}$ with S is given by the set of points $\{p \in S : \tilde{f}(p) \mp t_0 \overrightarrow{N_p} = p\}$. Substituting $\tilde{f}(p)$ by its value, we have $\mathcal{S}_{t_0} \cap S = \{p \in S : p + f(p)\overrightarrow{N_p} \mp t_0 \overrightarrow{N_p} = p\}$ which gives $\mathcal{S}_{t_0} \cap S = \{p \in S : f(p) = \pm t_0\}$. This is equivalent to say $\mathcal{S}_{t_0} \cap S = f^{-1}(\pm t_0)$. Thus level sets at instant t_0 are simply $\mathcal{S}_{t_0} \cap S$.
This property generalizes the *watershed transform* for 2D scalar fields. The watershed transform extracts morphology features of 2D scalar fields by crossing $\mathcal{S}$ parallel planes $z = constants$. In the 3D scalar field case, minima and maxima of f are obtained when S and $\mathcal{S}_{t_0}$ intersect tangentially. In case of non degenerate points, we obtain, at moment t_0, isolated points. And in case, of degenerate points we obtain sub-surface patches. After the detection moment of local minima (or maxima), circles are created and correspond to level sets of the function. When the inflation/deflation process continue in time, circles grow up on S until a moment in which an intersection between circles holds. At this moment, saddle points are obtained. When pursuing inflation/deflation process small time after, obtained saddle points split out and the previous circles merge together. Level circles propagate with time on S and the splitted points follow integral lines an describe the critical net of f over S (i.e., integral lines that are separatrices). Hence, the morphology of S is captured naturally by the inflation/deflation process.
In Figures 9 and 10, we represent the inflation/deflation process, at different moments, of function $f(x,y,z) = x^2 - y^2$ defined over the unit sphere S^2. Critical points of f and the critical net on S^2 appear naturally by the inflation/deflation process here. Critical net is formed by two orthogonal big circles on S^2 obtained from the intersection between S^2 with planes $x = 0$ and $y = 0$), see Figure $10(m)$.
We have seen in Section 3 that this function is not Morse and the study of *PGR* visualization implies four non degenerate points (2 maxima and 2 minima), and two degenerate points at north and south poles of the sphere. These poles are two (degenerate) saddle points. We retrieve here this result plus the critical net. Four Regions (stable and unstable components) representing Morse complex on the unit sphere are, thus, obtained.

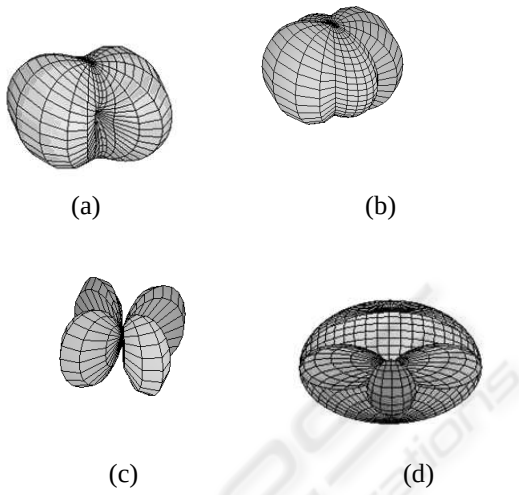

Figure 9: Inflation/Deflation process of function $f(x,y,z) = x^2 - y^2$ defined over the unit sphere S^2: In (a), surface $\mathcal{S}$ alone is depicted while in (b) *AUBL* visualization of S and $\mathcal{S}$ is shown. In(c), the completely deflated $\mathcal{S}$ is represented. In (d), a section showing the completely deflated scheme inside the unit sphere. The two intersection points of the unit sphere with the deflated surface are critical points of the same nature (minima or maxima).

Remarks.

- Under the inflation/deflation process, the scalar field is simply translated. Thus, the shape of the surface obtained from the *PGR* visualization of the field is the same. The surfaces is simply translated positively (inflation) or negatively (deflation), see Figure 8.
- In *AUBL* visualization, the shape of surface $\mathcal{S}$ depends continuously on the inflation/def-lation process, see Figure 10. This is due to the fact that the original surface S is curved. From another point of view, this is a remarkable fact, since it will give more flexibility to the user to work with the field under translations or homotheties. This will open other perspectives to study the fields with other approaches (constraint on field (i.e.,$\mathcal{S}$) curvature, ...). In medicine applications, the shape evolution, with time, of a pathological organ can be predicted with the inflation/deflation process (i.e, by translating the field by constants (time)). And hence consequences can be predicted, see Figure 11.

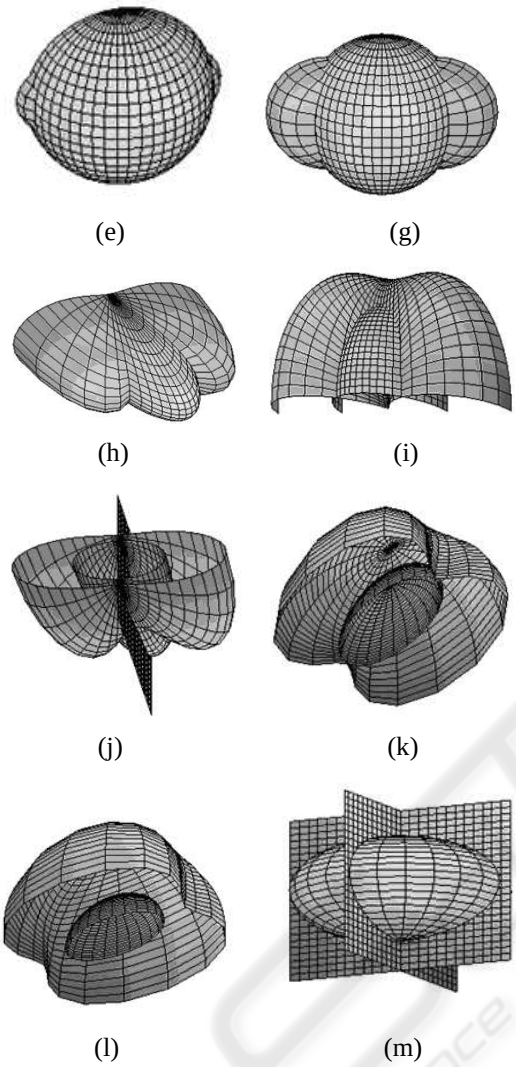

Figure 10: In(e), the beginning of the inflation process of $\mathcal{S}$. Unit sphere intersects the inflated surface at two created circles representing levels sets of f. In (g), the growing process of level sets (circles) appear clearly. In (h), the maximal growing of the two circles. Their intersection points are a saddles (north and south poles). In (i), each saddle point is splitted into 2 points to allow the previous circles to merge together in one curve that appear clearly. In (j), the splitted points follow the plane $x = 0$ and describe a big circle on the unit sphere. In (k), the ultimate intersection between S^2 and the inflated surface. In (l), pursuing inflation, we obtain a positive atmosphere around the unit sphere. In (m), the critical net corresponds to big circles obtained by the intersection of S^2 with planes $x = 0$, $y = 0$. Plane $y = 0$ corresponds to section in (d). Four Regions representing stable and unstable Smale-decomposition components are, thus, obtained.

- The curvature of the field (i.e., of surface $\mathcal{S}$) tends to 0 with inflation (positive translations). The classical methods do not approach fields from this point of view, since translations and homotheties do not have a significant importance from the Cartesian point of view. From our point of view this fact gives a coarse vision of the original field, see Figure 11. An application of *AUBL* to multi-resolution is conceivable from this point of view. Each resolution level corresponds to a translation value c. Coarse levels are obtained when c increases (inflation), and refined level appear when c decreases towards zero (deflation). The original surface is obtained for $c = 0$. Moreover, this multi-resolution process can be applied to the original surface S with function $f = 0$ (in this case we have $S = \mathcal{S}$) to produce multi-resolution models of surface S. We can also apply it to any function f to get multi-resolution models of surface $\mathcal{S}$. We can find a correspondence between inflation and the reduction process of the mesh, since the simplification process reduces the number of triangles and curvature tends to zero on larger regions. We can also find correspondence between deflation and refinement process, since this later increases the number of triangles and the curvature takes more precise values.

5 CONCLUDING REMARKS

We have presented two novel techniques *AUBL* and *PGR* that allow visualization of 3*D*-scalar fields in the Euclidean space R^3. *AUBL* and *PGR* techniques are coupled together to give a complete comprehensive representation of 3D scalar fields. We have pointed out other advantages of (*AUBL*,*PGR*) that allow the extraction of additional morphological features of the domain that may not be captured by classical tools. A method, based on *AUBL*, generalizing the watershed transform has been presented and detailed with an example. In our ongoing work, we will adapt *AUBL* technique for meshes and we will develop a visualizing tool that allow the user to interact with both *AUBL* and *PGR* techniques at the same time. Moreover, we will develop algorithms for the generalized watershed transform to extract morphology features of 3D scalar fields. We plan also to investigate the possibility of applying our approach in the visual data mining field. The idea is to enhance the segmental visualization technique (Ankerst, 2000) over a sphere divided into sectors.

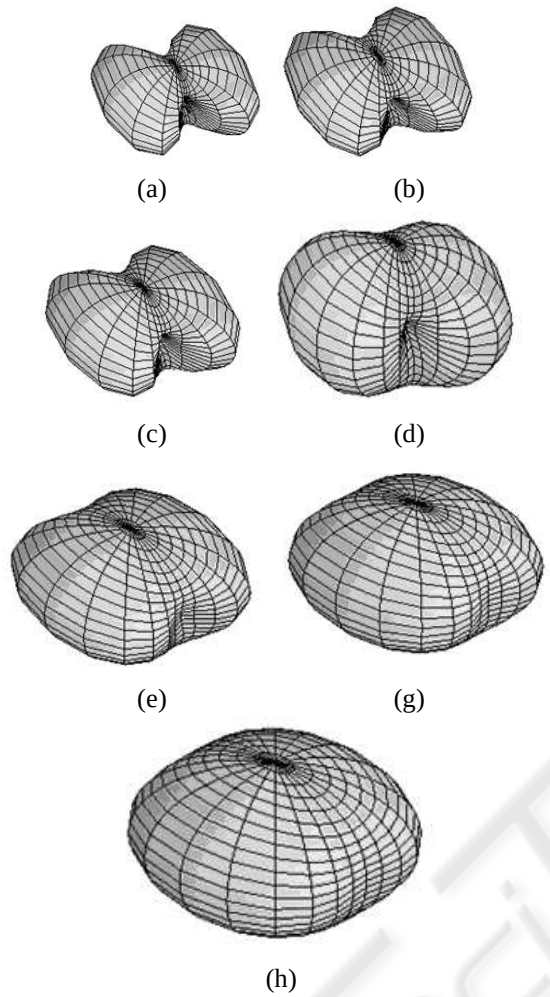

Figure 11: Evolution of surface $\mathcal{S}$ with inflation process. Size of $\mathcal{S}$ grows up and its curvature tends to 0 with time.

ACKNOWLEDGEMENTS

This work has been partially supported by a grant of the Polytechnic University of Valencia, Spain ("Programa de Apoyo a la Investigacion y Desarrollo 2006"), by the National Science Foundation under grant CCF-0541032, by the MIUR-FIRB project SHALOM under contract number RBIN04HWR8, by the MIUR-PRIN project on "Multi-resolution modeling of scalar fields and digital shapes", by the European Network of Excellence AIM@SHAPE under contract number 506766 and by the MCyT TIN2006-15265-C06-04 Spanish project. We kindly thank Dr. Fatiha M-Hammadi for the discussion we had on this work.

REFERENCES

Ankerst, M. (2000). *Visual Data Mining*. PhD thesis, Facultat fur Mathematik und Informatik der Lidwig-Maximilians-Universitat Munchen.

Bajaj, C. L., Pascucci, V., and Shikore, D. R. (1998). Visualization of scalar topology for structural enhacement. In *Proceedings of the IEEE Conference on Visualization '98 1998*, pages 51–58.

Bajaj, C. L. and Shikore, D. R. (1998). Topology preserving data simplification with error bounds. *Journal on Computers and Graphics*, 22(1):3–12.

Berger, M. and Gostiaux, B. (1972). *Gémoétrie Différentielle*. Collection U.

Edelsbrunner, H., Harer, J., and Zomorodian, A. (2001). Hierarchical morse complexes for piecewise linear 2-manifolds. In *Proc 17th Sympos. Comput. Geom.*, pages 70–79.

H. Edelsbrunner, J. Harer, V. N. V. P. (2003). Morse-smale complexes for piecewise linear 3-manifolds. In *Proc. ACM Symposium on Computational Geometry*, pages 361–370.

J.Toriwaki and Fukumura, T. (1975). Extraction of structural information from grey pictures. *Computer Graphics and Image Processing*, 7:30–51.

Mangan, A. and Whitaker, R. (1999). Partitioning 3d surface meshes using watershed. In *IEEE Transactionon visualization and Computer Graphics*, volume 5, pages 308–321.

Massey, W. S. (1977). *Algebraic Topology: an Introduction*, volume 56. Springer-Verlag.

Milnor, J. (1963). *Morse Theory*. Princeton University Press.

Nackman, L. R. (1984). Two-dimensional critical point configuration graph. *IEEE Transactions on Pattern Analysisand Machine Intelligence*, PAMI-6(4):442–450.

Peucker, T. K. and Douglas, E. G. (1975). Detection of surface-specific points by local paprallel processing of discrete terrain elevation data. *Graphics Image Processing*, 4:475–387.

Smale, S. (1960). Morse inequalities for a dynamical system. *Bulletin of American Mathematical Society*, 66:43–49.

Spivak, M. (1979). *A comprehensive introduction to differential Geometry*, volume 1. Houston, Texas.

Thom, R. (1949). Sur une partition en cellule associées a une fonction sur une variété. *C.R.A.S.*, 228:973–975.

Vincent, L. and Soille, P. Watershed in digital spaces: an efficient algorithm based on immersion simulation. In *IEEE Transactionon on Pattern Analysis and Machine Intelligence*, volume 13, pages 583–598.

Watson, L. T., Laffey, T. J., and Haralick, R. (1985). Topographic classification of digital image intensity surfaces using generalised splines and the discrete cosine transformation. *Computer Vision, Graphics and Image Processing*, 29:143–167.